Integrated geologic, geophysical, and petrophysical data to construct full field geologic model of Cambrian-Ordovician and Upper Cretaceous reservoir formations, Central Western Sirte Basin, Libya

Abdalla A. Abdelnabi[1], Yousf Abushalah[2], Kelly H. Liu[1], and Stephen S. Gao[1]

Abstract

The Cambrian-Ordovician and Upper Cretaceous formations, which are the main oil-producing formations in the central Sirte Basin, are structurally complex. The lateral and vertical heterogeneity of the reservoir formations is not well-understood, which negatively affects the performance of the reservoirs. We constructed efficient full-field static models that incorporate the lateral and vertical variation of those reservoir formations by integrating geologic and geophysical data. We determined lithology and reservoir properties by selecting appropriate petrophysical techniques that suit the available well data and overcome issues with unreliable well-log measurements. In the process of building structural models, defining and mapping the base of the Cambrian-Ordovician Gargaf Formation was very challenging because wells did not penetrate the basal formation, and the quality of the seismic data decreases with depth. Therefore, we applied techniques of adding isochore maps of the overlying Upper Cretaceous of the Bahi and Waha Formations to map basal contact and determine the thickness of the Gargaf Formation for the first time in the area. The constructed isochore maps showed the thickness variation and the distributions of the Bahi and Waha Formations and explained the influence of Gargaf paleotopography and faults on them. The fault models combined with facies and property models suggested an interconnection among the three main reservoirs. They also indicated that the quality of the Waha reservoir enhances as the lithology varies from limestones to calcareous sandstones, whereas the quality of the Gargaf reservoir was primarily controlled by fractures. The total estimate of the original oil in place with the largest contribution of hydrocarbon volume from the Waha Formation was 2.55×10^9 stock tank barrel. The created model with a fine-scale geocellular covering an area of 350 km^2 is unique to the study area and it can be updated and refined at any time with new data production and drilling activities.

Introduction

The Sirte Basin is among the world's top 20 petroleum provinces, and it is one of the four known sedimentary basins in Libya (Figure 1a). It covers a total area of 600,000 km^2 and is the richest and youngest sedimentary basin in the country, with known reserves of more than 43.1 billion barrels (Barr, 1972; Futyan and Jawzi, 1996; Wennekers et al., 1996; Coward and Ries, 2003; Craig et al., 2004; Abadi et al., 2008). The major structure of the Sirte Basin was developed between the Late Paleozoic and the Early Cretaceous, during which a continuous uplift formed the Sirte Arch. During the Late Cretaceous, extensional tectonics resulted in a partial collapse of the Sirte Arch and caused a system of horsts and grabens (Figure 1b; Klitzsch, 1971; Bellini and Massa, 1980; Van Houten, 1983; Ahlbrandt, 2001; Hallett, 2002). There are three primary reservoir formations: the Cambrian-Ordovician Gargaf, Upper Cretaceous Bahi, and Waha with a large variability in thickness and lithology in the study area (Figure 2; Cain, 2001). In spite of numerous studies, no consensus has been reached on the degree of connection among the different layers of the reservoirs and on the factors that distinguish these formations. As a result of its limited spatial distribution and thickness, the Bahi Formation contains the least hydrocarbon reserves. However, it is of significance because it acts as a good vertical and lateral reservoir conduit between the Waha and Gargaf reservoir units wherever it is present. Previous studies suggested that it is problematic to differentiate Bahi detritus and quartzitic materials from similar deposits found in either the Waha or Gargaf units (De Golyer and Macnaughton, 2010).

Integrating geologic, geophysical, and petrophysical data into one complete model of the whole field is an

[1]Missouri University of Science and Technology, Geology and Geophysics Program, Rolla, Missouri, USA. E-mail: aaakwd@mst.edu; liukh@mst.edu; sgao@mst.edu.

[2]University of Texas at El Paso, Geological Sciences, El Paso, Texas, USA. E-mail: yabushalah@miners.utep.edu.

Manuscript received by the Editor 22 December 2017; revised manuscript received 17 September 2018; published ahead of production 12 October 2018; published online 10 December 2018. This paper appears in *Interpretation*, Vol. 7, No. 1 (February 2019); p. T21–T37, 17 FIGS., 3 TABLES.
http://dx.doi.org/10.1190/INT-2017-0236.1.

important process to help better understand the complexity of reservoir formations, thereby facilitating significant gains in productivity in terms of identifying and managing reservoirs (Zou et al., 2006; Denney, 2013; Adeoti et al., 2014). It provides reservoir engineers with a reliable and comprehensive basis upon which they can simulate and manage reservoirs (Al-Harbi et al., 2013; Karamitopoulos et al., 2013). In general, however, combining these various forms of data represents a significant challenge, mostly because of the fact that reliable integration requires a comprehensive understanding of the inherent uncertainties of the numerous components in a given geologic system (Hosseini et al., 2012; Kamali et al., 2013; Musa et al., 2013; Rodríguez Torrado et al., 2015). Because the availability and variability of well data that were acquired by different companies in different years and quality of seismic data, it was required to use certain analysis techniques and data enhancement to overcome data limitations. Applications of frequency enhancement and filtering of seismic data on some oil fields in Libya, for example, demonstrated the importance of data conditioning to illuminate some of the unrevealed geologic features (Hamarbatan et al., 2006; Abushalah and Serpa, 2016, 2018; Abdelnabi et al., 2017). In a previous study (Abdelnabi et al., 2017), the authors used frequency enhancement and curvature attributes to identify minor faults in the study area and the distribution of the fractures in the Cambrian-Ordovician reservoirs. Here, we present a study of such an integrated approach using a combined data set from the RG-oil Field in the Sirte Basin in Libya. This case study uses a method by which a comprehensive blend of geologic, geophysical, petrophysical, reservoir engineering information, and the accompanying interpretations are linked in one static model. The modeling approach presented here is unique to the study area. One of the aims of this study is to characterize the heterogeneity of the main producing formations in the study area. The workflow of the construction of the full field static reservoir model of the RG-oil Field is illustrated in Figure 3.

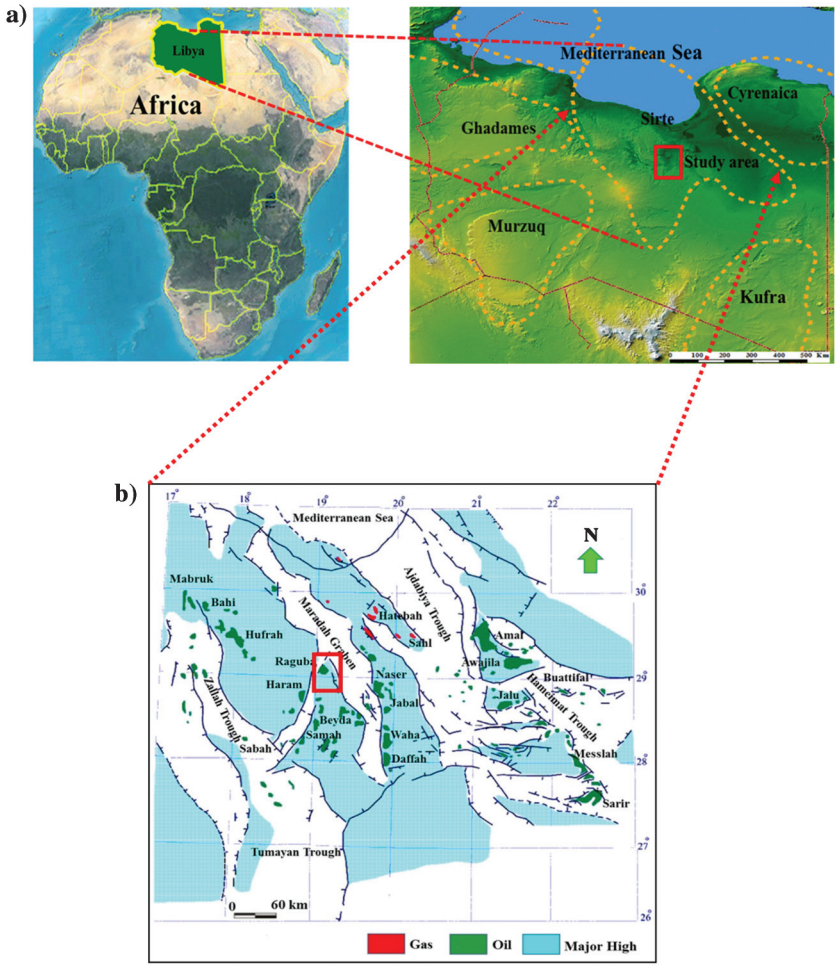

Figure 1. (a) Location map of the study area as indicated by the red rectangle in the Sirte Basin, Libya. (b) A structural map showing the main structural features affecting the sedimentation pattern in the study area. The blue areas represent major highs, the red areas represent gas field distribution, and the green areas represent oil fields (modified after Rusk, 2001).

Geologic background and database

Regional geologic setting and petroleum system

The RG-oil Field is located in the west-central part of the Sirte Basin (Figure 1). The major structural features that have affected sedimentation in this area include four northwest–southeast-trending structures (Van Houten, 1980; Anketell, 1996; Schroter, 1996), which are the Zallah and Tumayan Troughs to the west, the Beyda Platform in the central part of the area, and the Maradah Graben to the east (Parsons et al., 1980; Mansour and Magairhy, 1996; Capitanio et al., 2009). All platforms in the region are covered by limestone and remained relatively stable throughout the Early Paleocene. However, the shale-filled troughs continued to subside and deepen to the north particularly along the Ajdabiya trough to the present day (Gumati and William, 1985; Baric et al., 1996; Belhaj, 1996; Heselden et al., 1996; Johnson and Nicoud, 1996). The stratigraphy of the Sirte Basin was divided into four megacycles: Paleozoic, Triassic to Early Cretaceous, Late Cretaceous to early Oligocene, and Oligocene (Montgomery, 1994). The cycles characterize stages of pre-, syn-, and postrift sequences. The Cambro-Ordovician nonmarine clastics from the oldest megacycle (a prerift sequence) are represented by the Gargaf/Hofra sandstone, which is underlain by a Precambrian unconformity and overlaid by late Permian or Triassic unconformity. The sequence is characterized by tightly cemented sedimentary quartz-

ite, which is enhanced by fractures to form a secondary reservoir in the study area (Ahlbrandt, 2001). The second cycle is dominated by alluvial deposits of the Nubian Formation, which is not encountered by wells in the study area. The Late Cretaceous Bahi, Waha, and Sirte Formations (syn-rift sequences) characterize the third megacycle in the Sirte Basin, representing reservoirs and a source rock in the study area, respectively. The Bahi Formation contains a conglomerate of rounded pebbles with poorly sorted sandstones, siltstones, and shale representing nonmarine fluvial deposits. The Waha Formation is developed around preexisting high topography, and its lithology varies from open marine to nearshore deposits (Hallett, 2002).

The dominant petroleum system in the study area is called the Sirte-Zelten. The thick Upper Cretaceous marine shale, which is part of a synrift sequence, contains the principal source rocks, whereas the reservoirs are shallow-marine clastics and carbonate deposits situated on horst blocks (Hamyouni et al., 1984; Gumati and Schamel, 1988; El-Alami, 1996; Hallett and Ghoul, 1996; Boote et al., 1998). Subsidence in the basin occurred at different rates, and four major phases of extension impacted deposition throughout the basin (Gumati and Nairn, 1991; Roohi, 1996a, 1996b; Sinha and Mriheel, 1996). The reservoirs were formed by the onlap of Cretaceous rocks (Bahi and Waha Formations) onto the Paleozoic Gargaf, which might influence the limit and distribution of reservoir facies in the study area. The oil migration occurred from the early Oligocene to the late Miocene age where lateral migration through Bahi carrier beds and vertical migration along the bounding faults from troughs to the Gar-

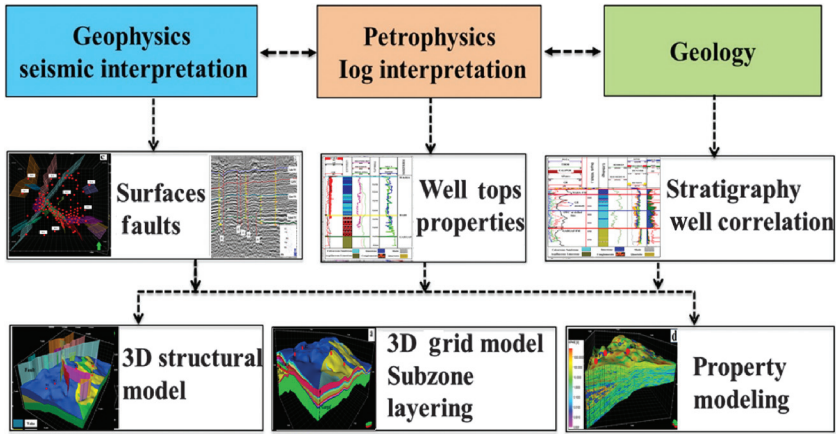

Figure 3. Model development workflow showing the process of integrated geologic, geophysical, and petrophysical data to construct a full field static reservoir model of the RG-oil Field using all the available data such as seismic, well log, and core description data.

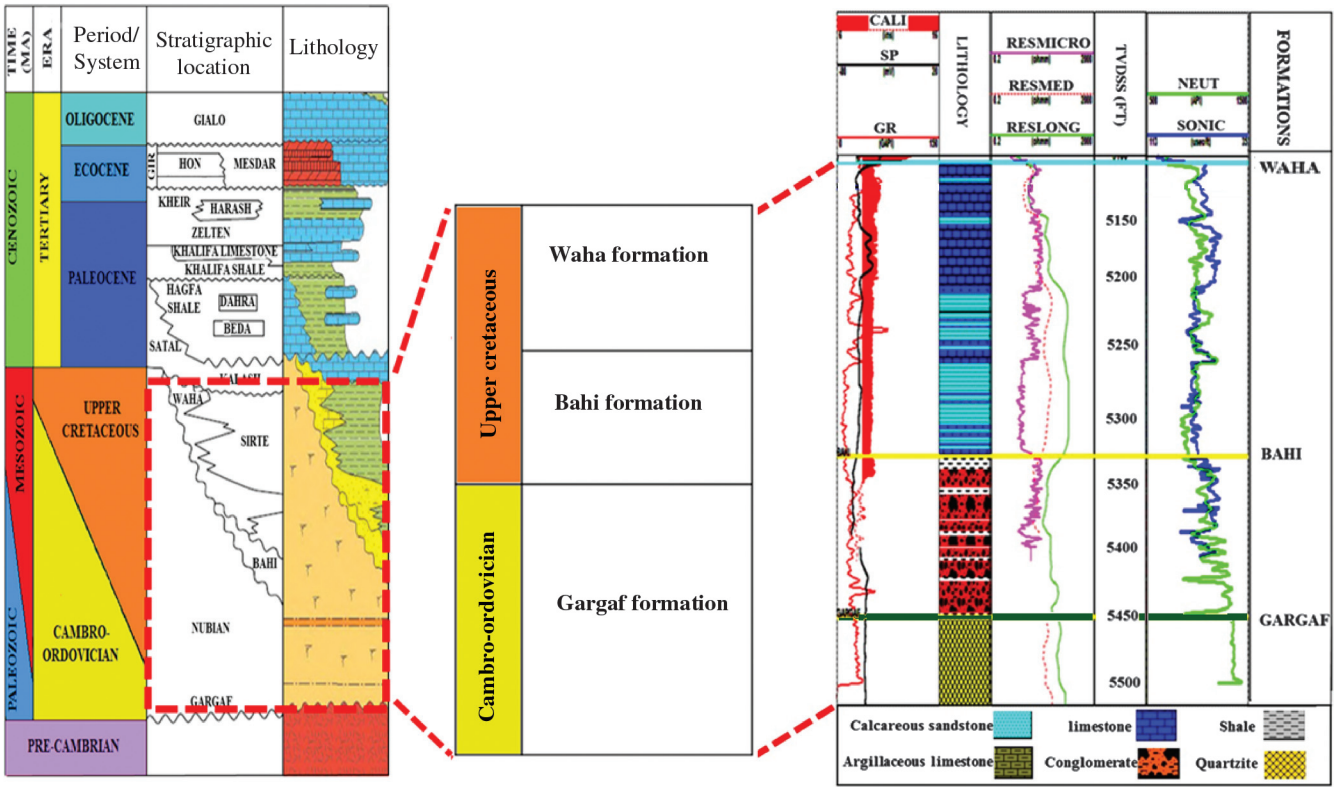

Figure 2. A stratigraphic-lithologic column of the central Sirte Basin (the left figure was modified after Barr and Weegar, 1972). The figure depicts the Cambrian-Ordovician and Upper Cretaceous reservoir formations in the study area. The Cambrian-Ordovician Gargaf and the Upper Cretaceous Waha and Bahi Formations are identified based on well logs and formation tops (right).

gaf, Bahi, and Waha Formations took place (Rusk, 2001; Hallet, 2002) The Hagfa Shale forms the caprock (Figure 2; Bonnefous, 1972; Baird et al., 1996). The trap is a large irregular domal structure that covers an area of approximately 25,000 acres. It is bounded on the west by a major northeast–southwest-trending normal fault with minor faults cutting the interior of the structure (Boweman, 1962; Hassan, 1971).

Data set

The seismic reflection data used in this study consist of 23 2D migrated lines covering an area of approximately 4000 km^2 and a 3D seismic cube covering an area of approximately 351 km^2. The 2D and 3D seismic data quality ranges from fair to good (Figure 4). Checkshot surveys used to tie the well tops to the seismic data are available for several wells. Data inquired by different companies in different years from 140 wells were also used for the study (Figure 5). The seismic-to-well ties were evaluated by constructing synthetic seismograms at well locations whenever sufficient sonic (DT), or sonic and density (RHOB) data are available. A total of 140 wells and core descriptions and quantitative analyses from 30 wells were available for the petrophysical study in support for the construction of properties modeling.

Methods

Petrophysical analysis

A petrophysical analysis was performed for 140 wells from inside and outside the study area. We estimated reservoir properties for 100 wells and made lithostratigraphic correlations for all 140 wells. We also used quantitative analyses of core samples from 30 of the wells to calibrate petrophysical properties. Different petrophysical techniques were selected to estimate the reservoir properties and lithology based on the vari-

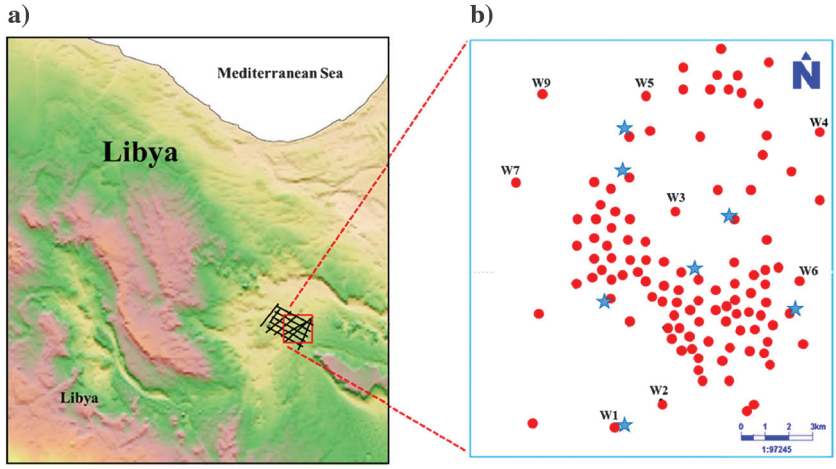

Figure 5. (a) Topographic map of Libya. The red box presents the area covered by the 3D seismic data, and the black lines are 2D seismic profiles. (b) Distribution of wells used in the study. The blue stars represent wells with check shots.

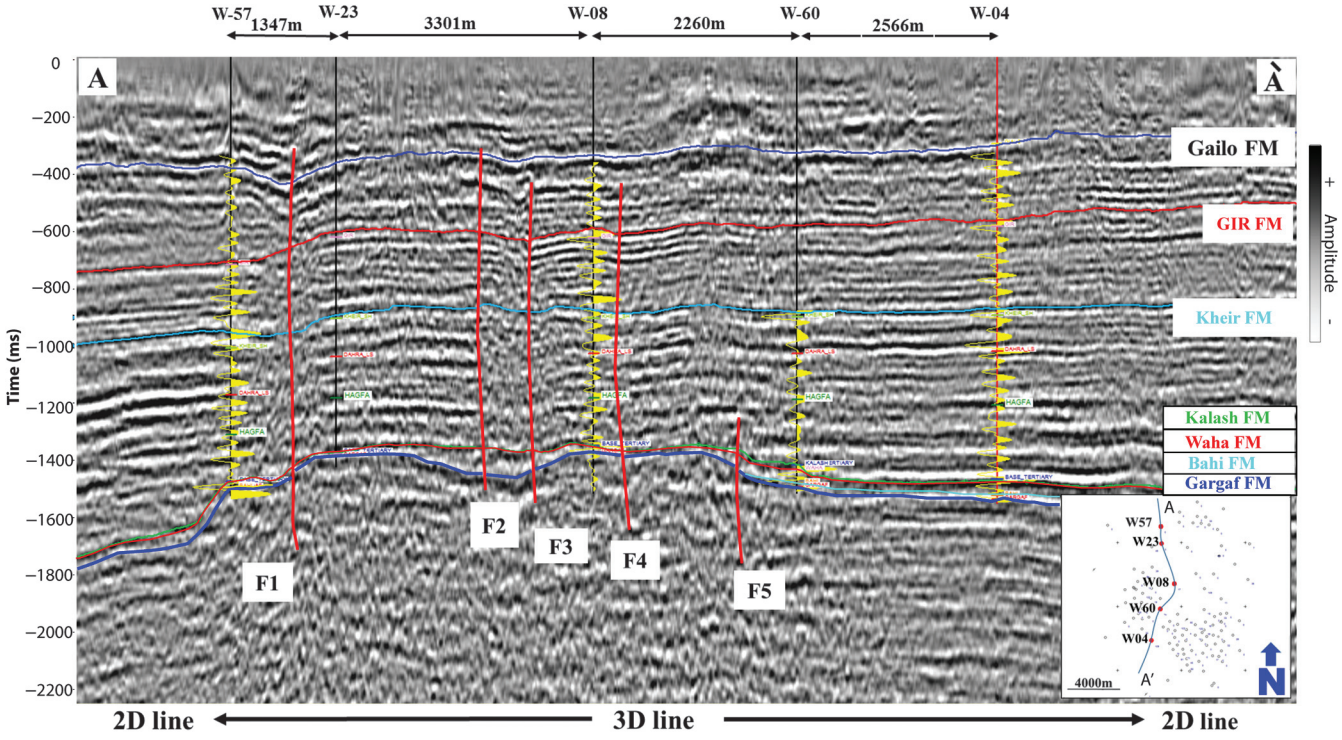

Figure 4. North–south seismic section showing the tie of 2D and 3D seismic data, seismic-to-well tie for well 57, well 08, and well 04 represented by the yellow trace on the seismic section. Also shown are major faults F1 and F2 and horizon interpretation of the main formations in the study area.

ability, uncertainty, and availability of well data as discussed below.

Determination of porosity, permeability, and water saturation

We used different petrophysical methods to estimate porosity for each specific well, depending on the presence of core and well-log data and whether the reservoir zone had significant shale content. For the newer wells that contain density logs, the density-neutron crossplot technique was adapted to determine the porosity and lithology. For the older wells that contain low shale, and the shale was concentrated in a distinct bed in the reservoir formations, sonic and neutron (NEUT) logs were used to estimate the porosity because there was no need to apply shale correction to porosity. For wells in which density logs were missing, the NEUT logs were only used if DT logs were not available. Although microlaterolog (MLL) logs were used to determine porosity in 10 wells with DT and NEUT logs, we did not use them because MLL logs are more sensitive to the common washout than DT and NEUT logs in these wells. The core-derived porosity in 15 wells was then used to calibrate the logs.

Because there was a variety of resistivity logs such as laterolog, normal and lateral, deep indication logs that were acquired in different years in the field, we generally used the shallow resistivity logs qualitatively to identify permeable beds, and the deep resistivity logs to compute water saturation. We used resistivity and spontaneous potential (SP) logs in all wells as indirect permeability indicators. The SP was used as a Boolean permeability indicator because the reservoir lithology is relatively shale-free, and SP is known to measure the electrical potential generated at the interface between permeable and impermeable beds (Asquith et al., 2004). We also used the separation of the shallow and deep resistivity readings as another permeability indicator. Two shallow-reading electrode pad resistivity devices, microlog and microspherically focused log (MSFL) for six old wells, were used as permeability indicators. Micrologs record two simultaneous measurements, the micronormal (MNOR) and the microinverse (MINV) curves. The MNOR log reads approximately 2 in into the formation, and the MINV log reads approximately 1 in into the formation, and the permeability is indicated when the log readings are different. MSFL were available and were used as qualitative permeability indicators. We used the deep resistivity measurements (Rt) to estimate water saturation (Sw) that was calculated from the Archie equation. We also used the resistivity logs and core data to determine the depth of oil-water contact (OWC) and gas-oil contact (GOC) at the time of drilling (original contacts).

Lithology determination

We identified the rock type and established lithostratigraphic correlations in the wells directly from wireline, cutting descriptions, and mudlogs in a final well report. We used the density-neutron crossplot as a primary method in the new wells (where density logs were recorded) to estimate the lithology and to distinguish limestone from calcareous sandstone in the Upper Cretaceous Waha Formation. We identified quartzite and rare shale in the Gargaf Formation and conglomerate/boulder beds and siliceous sandstones in the Bahi Formation. We also identified limestone, calcareous sandstone/sandy limestone, and thin shale in the Waha Formation. Argillaceous and sideritic limestone were also present in the Waha Formation, but in few wells. Based on the observation of porosity variations, the siliceous sandstone facies of the Bahi Formation was distinguished from quartzite of the Gargaf Formation by an increase in porosity, and the boulder beds of the Bahi Formation were distinguished from the quartzite facies of the Gargaf Formation by a decrease in porosity.

Because of issues with gamma ray (GR) logs as discussed below, shales were estimated as a Boolean indicator using resistivity, SP, spectral GR, and/or neutron logs during lithology determination. The GR appears to be affected by uranium, which is unrelated to the clay mineral or shales in the reservoir formations. The high GR anomaly in well 1 (Figure 6), for instance, is not consistent with the other well-log responses including thorium (Th) and potassium (K) curves, and hence it does not indicate the presence of shale in the reservoir formation. Because it is very difficult to know how much uranium is in GR logs and how much of it is related to fluid movements in the logs, we used Th and K and/or computed GR from spectral GR as shale indicators. We also defined the shale as of very low porosity with indications of impermeability on the SP logs. We used cutoffs on the resistivity, neutron, and DT logs to distinguish shale from quartzite and siliceous sandstone in the Bahi and Gargaf Formations. Shales in the Bahi and Gargaf Formations are characterized by spikes toward high porosity on neutron logs.

Seismic horizon and fault interpretation

The seismic interpretation was started by tying the 2D and 3D seismic data (Figure 4). Then, seismic data were tied to well data using approximately 60 wells that have sonic data in which 30 of them contain density logs. The ties were evaluated by constructing synthetic seismograms at well locations (Figure 4). Those synthetic seismograms were generated using sonic and either measured or estimated density logs (when density logs were missing) using Gardner's equation (Gardner et al., 1974). The seismic-to-well tie was good, and the best ties were obtained with the 3D survey.

The horizon interpretation of the main reservoirs, including the Gargaf, Bahi, and Waha Formations, and other formations, such as Kalash, Kheir, Gir, and Gailo, were carried out using the 2D and 3D seismic data (Figure 4). Shallow horizons were easy to track over the study area because they represent strong reflection contrasts with better seismic resolution. Data quality deteriorates with increasing depth and increases the uncertainty of the interpretation of the deep horizons

(Abdelnabi et al., 2017). Nevertheless, there is enough well control to constrain the interpretation and produce accurate structural maps of the deep horizons. We also interpreted faults using 2D and 3D seismic data in which the minor faults were identified from frequency-enhanced seismic data (Abdelnabi et al., 2017). We picked the faults in every inline and crossline. It is crucial to identify the faults and understand their relationship to the reservoir. We identified 40 faults in the study area (Figure 7a), and only 20 faults were determined to be connected to the reservoir network (Figure 7b). Some of those faults are displayed in Figure 4. Finally, we used average velocity from well data and performed time to depth conversion for the interpreted horizons of the reservoir formations.

Structural, facies, porosity, and permeability modeling

We constructed structural and isochore maps using the seismic, well log, and core data to define the top surface, thickness, and distribution of each of the three reservoir formations in the study area (Figures 8, 9, and 10) and provide a framework for the 3D static model (Figure 11). Because the basal of the Gargaf Formation was not penetrated in the wells, the isochore map of the Gargaf (Figure 8b) was created by adding the total isochores maps of the overlying Upper Cretaceous Bahi Formation and Upper Cretaceous Waha Formation (Figures 9b and 10b). Subsequently, the identified faults and structural surfaces were imported into the structural model and were refined to produce the best representation of the seismic and well data (Figure 11). The structural model comprises three main zones representing the three main reservoirs. The Cambrian-Ordovician Gargaf zone was then divided into 12 subzones based on lithologic and petrophysical variations, whereas the Upper Cretaceous Waha zone was divided into 10 subzones based on the stratigraphy. Because the Upper Cretaceous Bahi Formation is a heterogeneous succession with variable thicknesses and lateral extents, we represented the Bahi Formation as one reservoir zone as shown in Figure 12. The subzone thicknesses of each formation were chosen to best capture the vertical heterogeneity that the petrophysical properties exhibit. The final process of structural modeling was layering in which a minimum cell thickness of 1 m was chosen as a threshold to prevent accumulation of thin cells at the unconformity during the layering process. The cell layers were generated based on proportional cell thickness to define the final vertical resolution of the grid model, in which a constant number of cell layers was defined in each subzone. The 3D grid has a horizontal dimension of 16.9 km along the x-axis and 20.8 km along the y-axis, covering a surface area of 351.52 km^2. We use a corner-point 3D grid to create grids based on the fault and structural models. The areal cell size for the model is chosen as 100 m × 100 m, and the thickness of the cells is proportional to the overall zone thickness. The resulting static model has a fine-scale dimension of 248 × 265 × 466 (30.6 million cells).

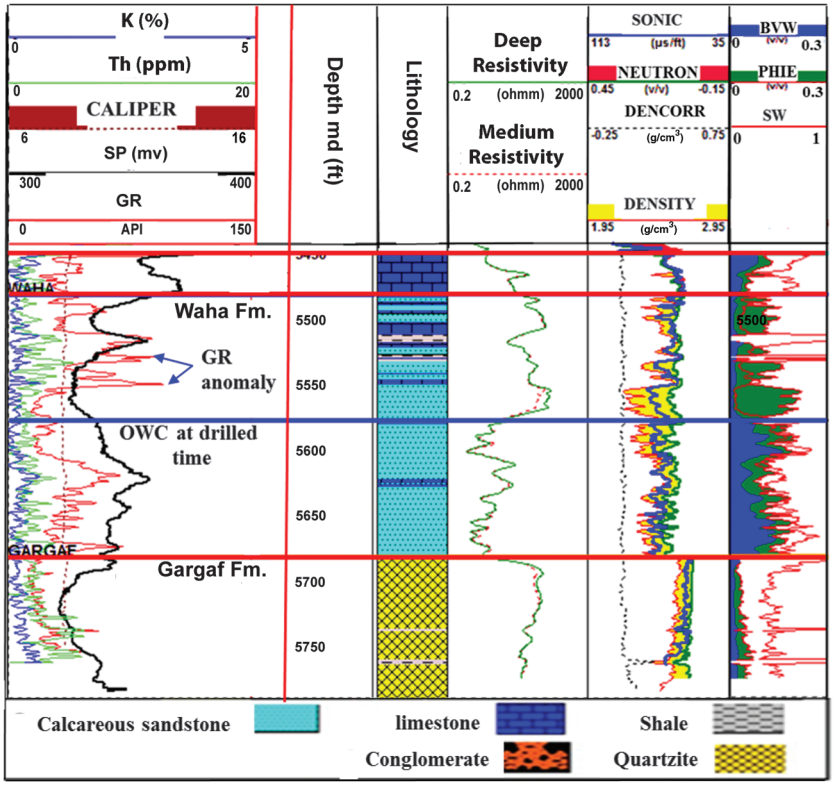

Figure 6. The left tracks show lithology estimation within the reservoir formation of the Upper Cretaceous Waha Formation and Cambrian-Ordovician Gargaf Formation of typical well 100. It also shows the anomalies in GR logs and how there is no support to interpret the high spike in the GR log as shale in other lithology logs such as the Caliper and SP logs. The right tracks show the logs used to calculate and determine the OWC, porosity, bulk volume of water (BVW) and water saturation (SW).

The identified facies of the Gargaf, Bahi, and Waha Formations were then populated across the constructed 3D structural model using the sequential indicator simulation (SIS) statistical method (Figure 13). The SIS is a widely used technique for categorical variable models (e.g., Journel and Isaaks, 1984; Journel and Alabert, 1988). The SIS algorithm uses a random path through all of the grid nodes to avoid artifacts. It then uses a kriging algorithm to estimate the conditional distribution of each facies type at each closet grid node, which is randomly selected to draw the simulated value from. The process repeats, and each time the original and previous simulated values were added in the estimation processes. In the process of generating the facies model, a sample isotropic variogram with appropriate lags and hori-

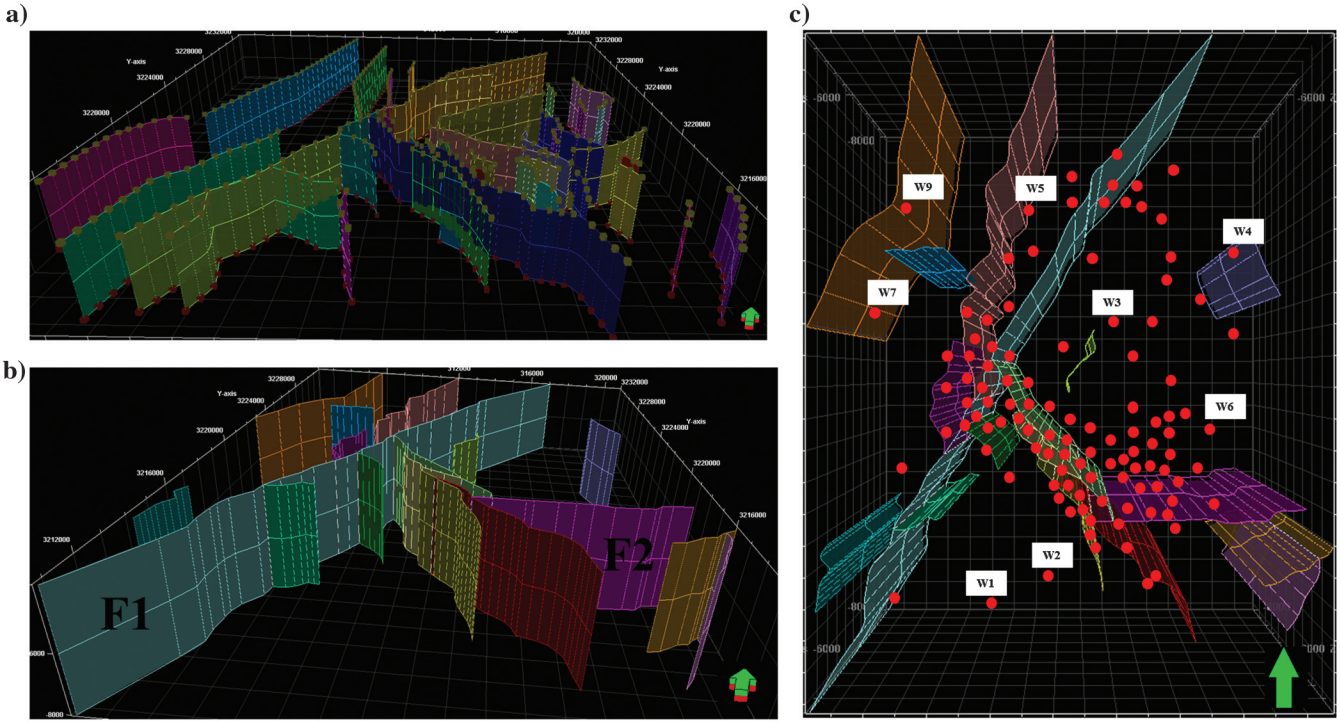

Figure 7. Fault identification from seismic data. (a) The 40 faults identified in the study area and (b) the 20 selected faults used in the full static model including two major faults (F1 and F2). (c) A top view showing the fault model used in the static model and the distribution of the wells.

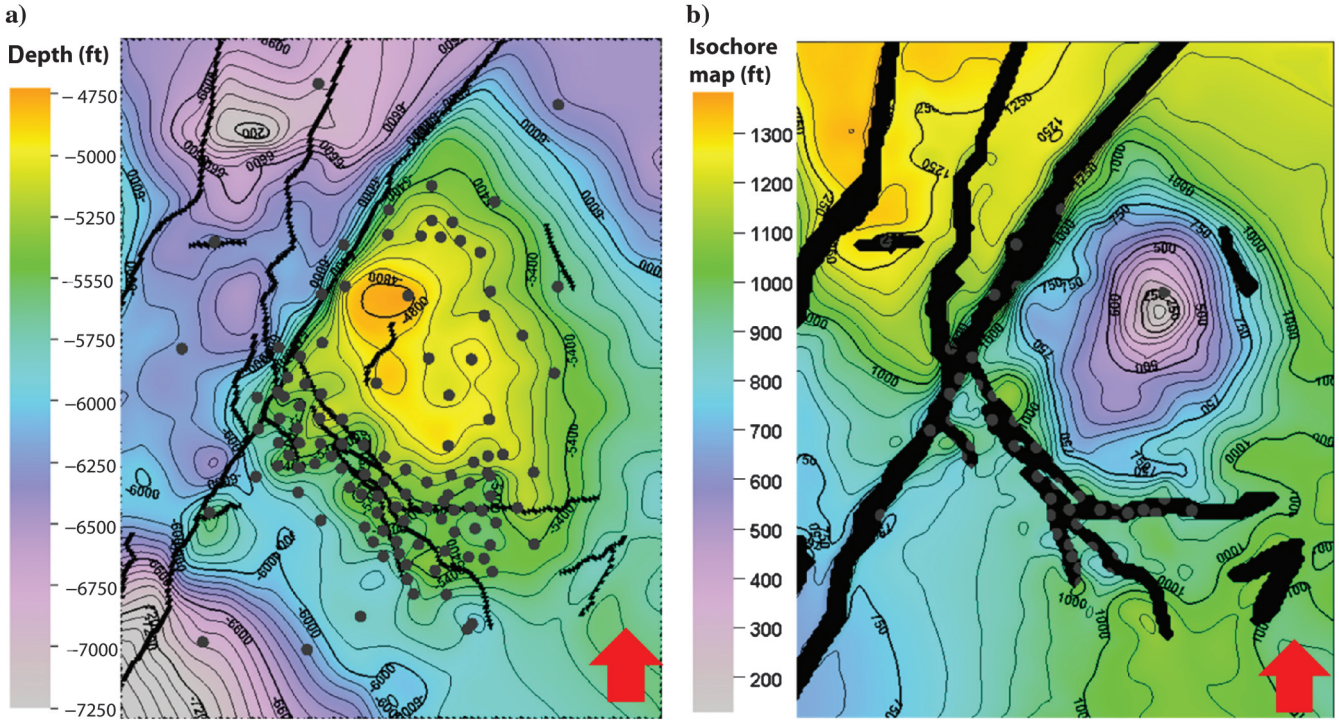

Figure 8. Structural contour map and isochore map based upon seismic, wireline log, and core data of the Cambrian-Ordovician Gargaf Formation. (a) A depth structure map showing the main structural features in the study area, in which the black lines represent faults and the black dots represent the wells' location and distribution. (b) Isochore map showing the thickness distribution of the Cambrian-Ordovician Gargaf Formation.

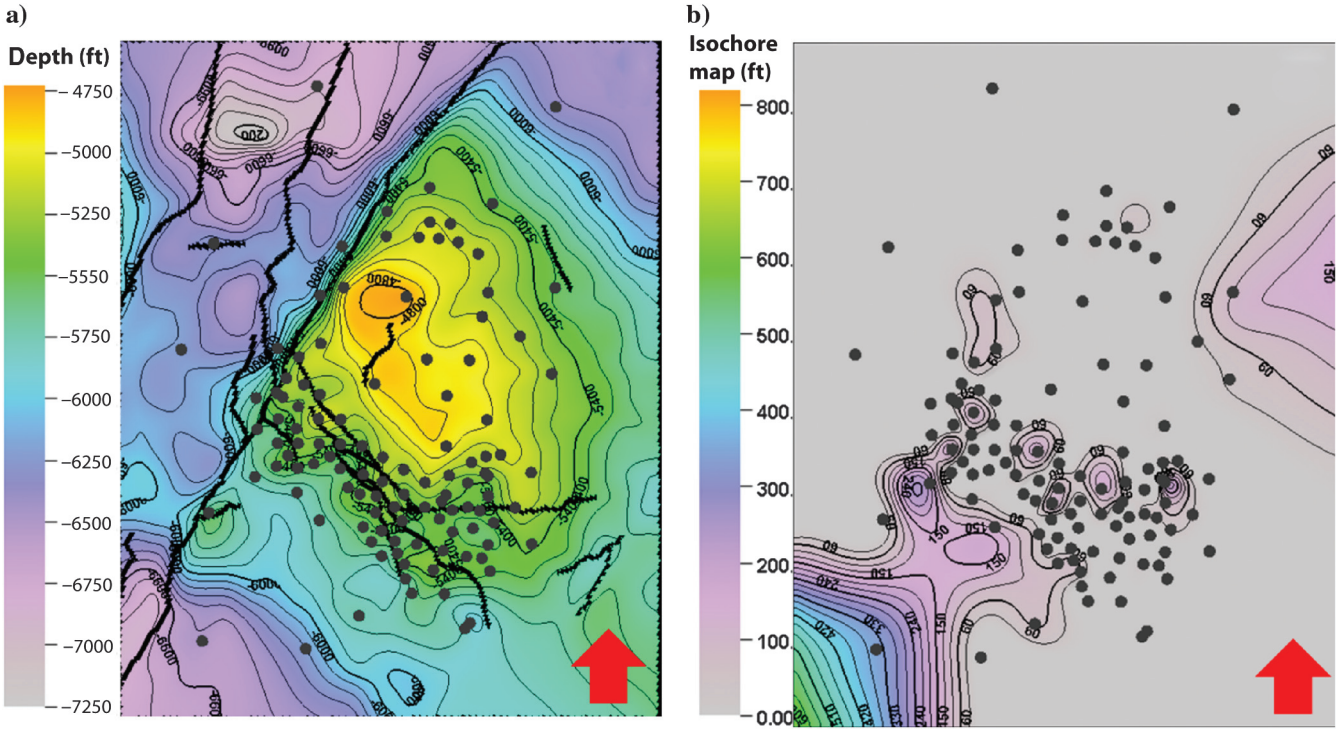

Figure 9. Structural contour map and isochore map based upon seismic, wireline log, and core data of the Cretaceous Bahi Formation. (a) A depth structure map showing the main structural features in the study area, in which the black lines represent faults and the black dots represent the wells' location and distribution. (b) Isochore map showing the thickness distribution of the Cretaceous Bahi Formation.

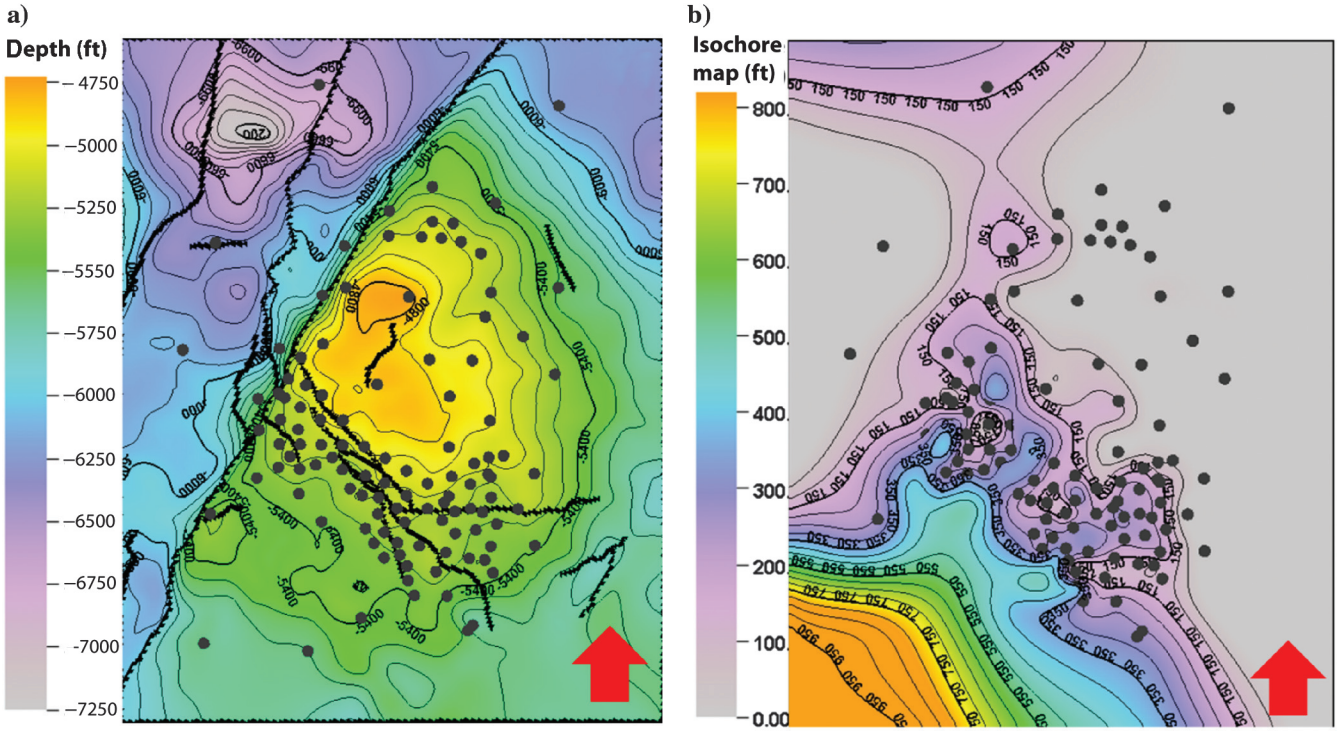

Figure 10. Structural contour map and isochore map based upon seismic, wireline log, and core data of the Upper Cretaceous Waha Formation. (a) A depth structure map of the top Waha reservoir showing the main structure in the study area, in which the black lines represent faults and the black dots represent the wells' location and distribution. (b) Isochore map showing thickness distribution of the Upper Cretaceous Waha Formation.

zontal search radius for each facies in 23 zones was chosen to represent the vertical and horizontal variations of the lithofacies, assuming the lithology of the Bahi and Waha Formations is changing from northeast to southeast parallel to the Gargaf paleohigh. The variogram type was classic, in which half of the average squared difference between the paired data values was calculated, whereas the variogram model was a spherical or exponential curve. The resultant facies model constructed for the three formations was used as a reference to assign porosity and permeability values as discussed below (Figure 13).

We used distinct porosity log and deep-reading resistivity log technologies in addition to quantitative analyses of the petrophysical properties of core samples to determine porosity and permeability values as discussed in the petrophysics section. After calibration of the petrophysical values with the available core data and upscaled them, the porosity and permeability were modeled using a sequential Gaussian simulation (SGS) model (Figures 14 and 15). The SGS is similar to SIS except using indicator kriging to estimate conditional distribution in SIS. It uses kriging to estimate the mean and the standard deviation. The model was defined by the experimental variogram with the same search parameters as those used for facies modeling.

Net-to-gross ratio and volumetric estimations of the hydrocarbon resources

We chose the net-to-gross (NTG) model in accordance with a net and pay zone that comprises ones and zeros. Ones represent layers that passed the cutoffs (permeability >= 0.01 md) and are treated as a reservoir, whereas zeros represent layers that failed the cutoffs and are treated as a nonreservoir. After testing the method, we found that the same variograms used to distribute the porosity grid can be successfully used to distribute the NTG grid (Figure 16).

We calculated water saturation using well-log data with emphasis on the Rt logs and then matched on a foot-by-foot basis and corrected for structural elevation based on the computed saturation-height gradient observed in the wells. The height above OWC and GOC was calculated using geometric modeling based

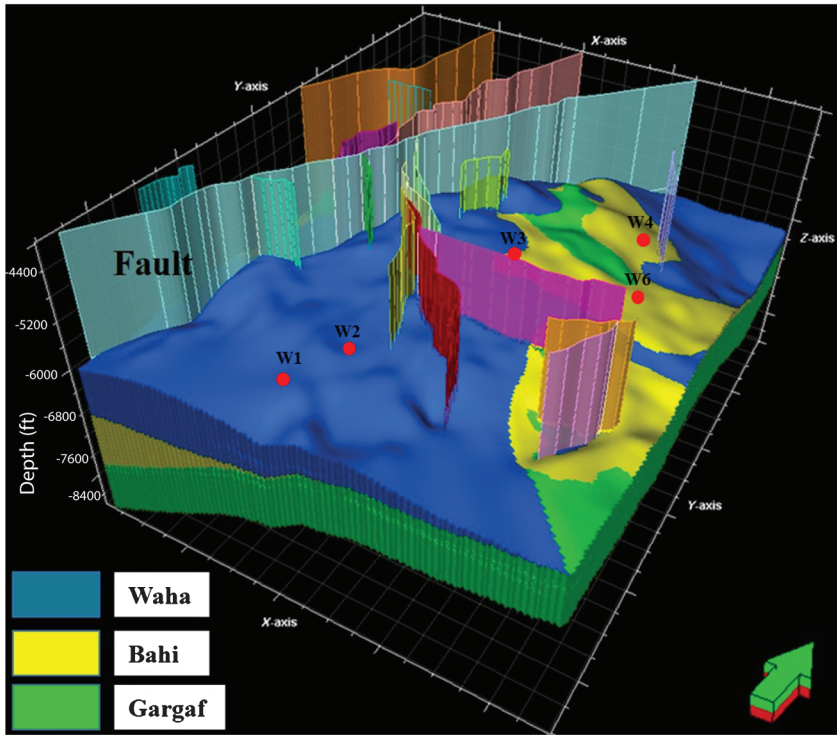

Figure 11. The 3D structural model of the study area showing selected Cambrian-Ordovician and Upper Cretaceous horizons. The faults are represented as fault polygons in the 3D structural model.

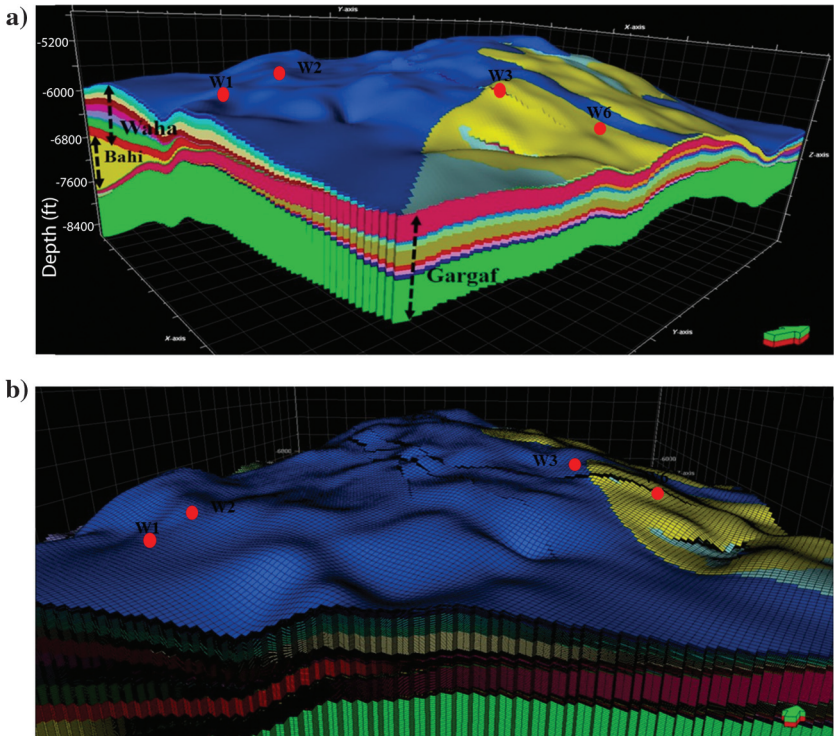

Figure 12. The 3D structural and grid models showing the subdivision of the Cambrian-Ordovician and Upper Cretaceous reservoir formations. The Upper Cretaceous Waha is divided into 10 subzones, and the Upper Cretaceous Bahi is considered one zone. (a) The 12 subzones of the Cambrian-Ordovician Gargaf Formation. (b) Added layers in the Cambrian-Ordovician and Upper Cretaceous reservoir formation subzones.

on the previously identified OWC and GOC contacts from resistivity logs and core data. Then, the J function was empirically computed as a function of square root of permeability to porosity and above OWC and GOC, which was then used to estimate water saturation. After all the fluid contacts and necessary models, including structural, facies, porosity, permeability, NTG ratio models, and water saturation, were established in Figure 17, and we estimated the hydrocarbon pore volume and original oil in place (OOIP) for each formation of the Cambrian-Ordovician and Upper Cretaceous reservoirs in the full field geologic model (Table 1).

Results and discussions

Interpretation of fault model

Forty faults were identified from the seismic reflection data (Figure 7a). To simplify the model, we excluded from the structural model the faults that are not connected to the reservoir fault network. Consequently, 20 of the 40 faults were used to construct fault polygons that were imported into the geologic model (Figure 7b and 7c). Two major faults F1 and F2 were responsible for the formation of the structural closure in the study area. The major fault (F1) is located on the west side of the field, having a northwest–southeast trend with a net throw of approximately 250 m toward the west. The fault separates a platform structure to the east from the graben structure to the west. In addition, it effectively seals the structure on the west side of the producing area and appears to diminish in the Hagfa Shale at the top of the reservoir. A northeast–southwest major fault (F2) with a throw of 130 m toward the east also appears to seal the structure on the east side of the reservoir (Figure 7b). The minor faults that cut the interior of the structure and subparallel to the major faults enhance the reservoir communication in most of the field. The throws of the minor faults range from 20 to 100 m. Previous studies suggested that these faults formed in response to extensional tectonics during the Late Cretaceous age (El-Ghoul, 1996; Mansour and Magairhy, 1996). The faults appear almost vertical, in particular within the reservoir units (beneath the Kalash Formation) as shown in Figure 4, which simplified the fault modeling.

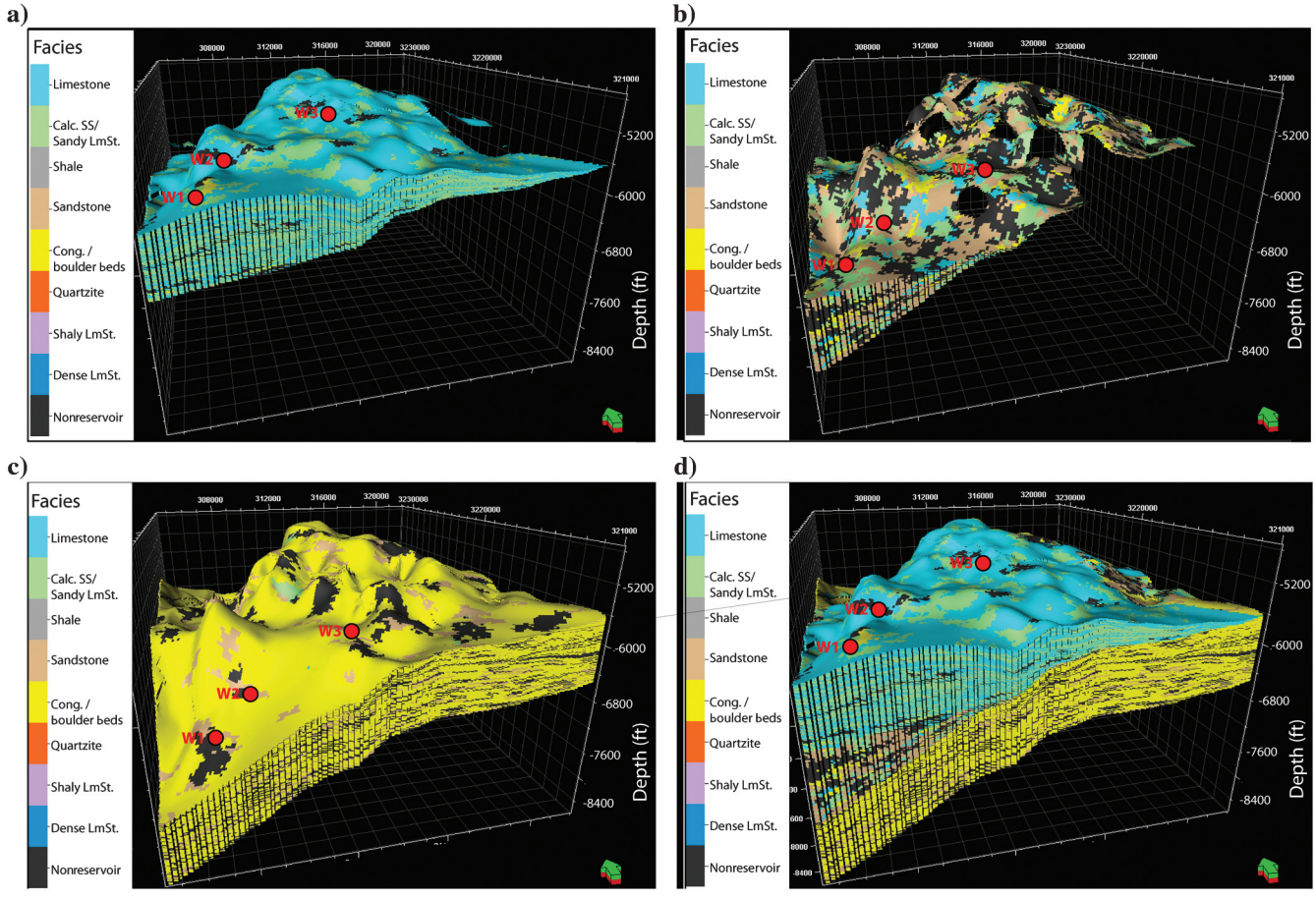

Figure 13. The 3D facies model of the Cambrian-Ordovician and Upper Cretaceous reservoir formations built using the SIS method. (a) The 3D facies model of the Upper Cretaceous Waha Formation, (b) 3D facies model of the Upper Cretaceous Bahi Formation, (c) 3D facies model of the Cambrian-Ordovician Gargaf Formation, and (d) full-field 3D facies model of the Waha, Bahi, and Gargaf Formations.

Structural interpretation and modeling

The defined tops and thicknesses of the reservoir formations that combined with faults provide crucial information about the reservoir productivity area, distribution, and connectivity, and they were used to construct a structural framework for property modeling. The Cambrian-Ordovician Gargaf Formation is the second reservoir unit with a widespread distribution in the study area (Figure 8a and 8b). It is overlain unconformably by clastics of the Bahi Formation or clastics and carbonates of the Waha Formation. The Gargaf Formation thins on the crest of the structure and thickens elsewhere, particularly toward the north–northeastern and southeastern area (Figure 8b). The variation of the Gargaf thickness suggests that the Gargaf paleostructure in the central area was formed before the Late Cretaceous transgression, which agrees with previous studies (Hallett, 2002). This also suggests that fractures of the Gargaf Formation might have formed during the formation of the Gargaf domal structure before Cretaceous faulting. The latter event probably enhanced the fracture system in the faulted areas.

The Bahi reservoir unit is the least important of the three units due to its reduced thickness that ranges from 0 to 55 m and its patchy distribution within the structural closure. However, it is a good reservoir communicator between the underlying Gargaf Formation and overlying Waha Formation as discussed in the facies model section. We determined the thickness of the Bahi reservoir unit to be approximately 46 m (150 ft), with a general increase toward the southwestern part of the study area where the Bahi Formation recorded a maximum thickness of 76 m (250 ft) (Figure 9b). We believe that the undulation of the Gargaf paleostructure and the active Cretaceous faulting created high and low areas were responsible for the thickness variation and patchy distribution of the Bahi reservoir. This can be indicated by elongated depressions of thick deposits in the faulted area (Figure 9a and 9b) and a large variation in thickness between some of the adjacent wells.

The Upper Cretaceous Waha Formation constitutes the upper and major reservoir in the study area. The constructed structural and isochore map delineated the thickness and distribution of the Waha Formation (Figure 10a and 10b). We found that the thickness of the Waha Formation ranges from 61 m (200 ft) on the north side of the study area to more than 244 m (800 ft) and largely dominant distribution in the southwestern

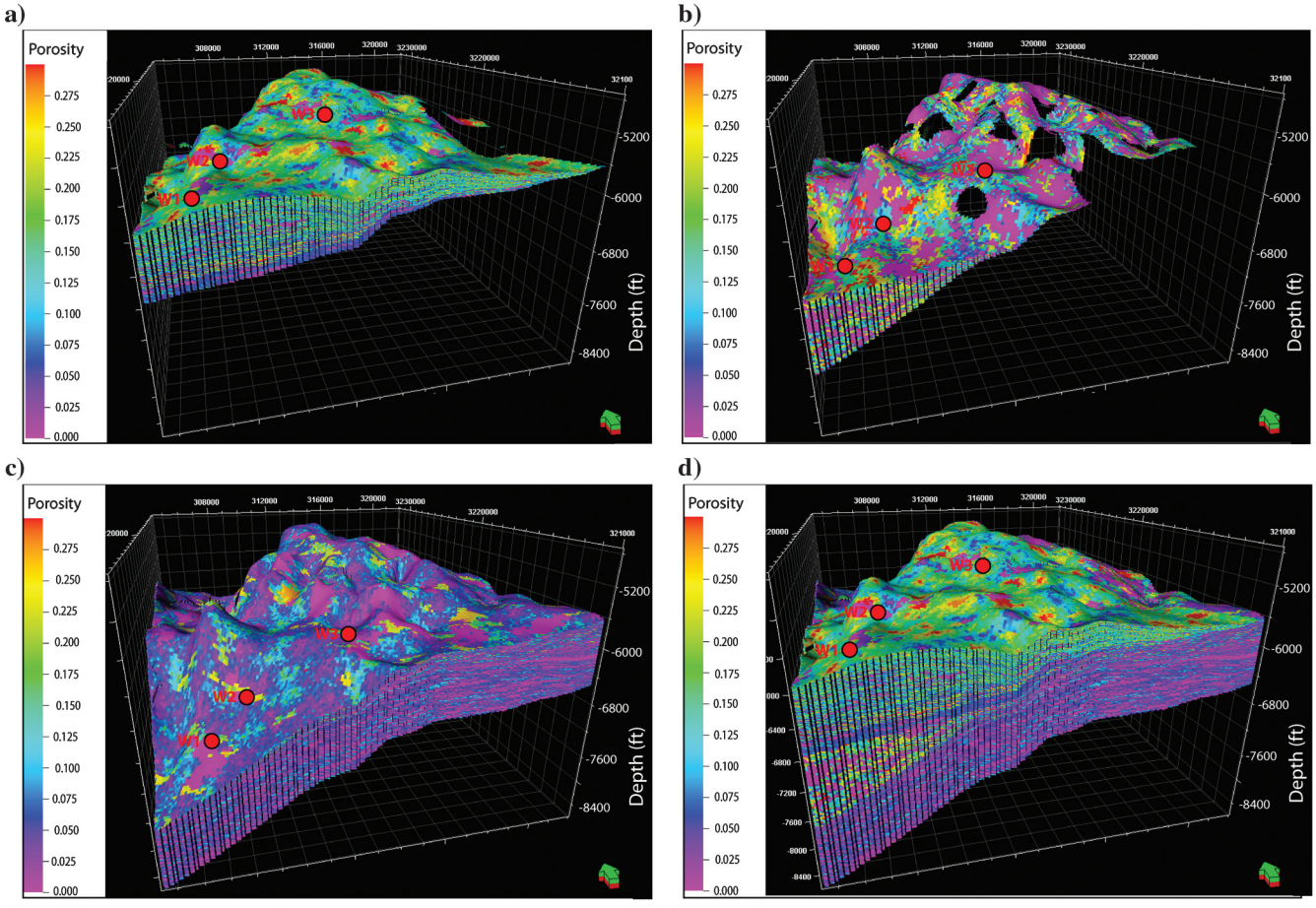

Figure 14. A 3D porosity model of the Cambrian-Ordovician and Upper Cretaceous reservoir formations using the SGS method. (a) The 3D porosity model of the Upper Cretaceous Waha Formation, (b) 3D porosity model of the Upper Cretaceous Bahi Formation, (c) 3D porosity model of the Cambrian-Ordovician Gargaf Formation, and (d) full-field 3D porosity model of the Waha, Bahi, and Gargaf Formations.

part of the study area. As shown in Figure 10b, the Waha Formation is absent in the northeastern area, apparently because the marine deposits of the Waha Formation are restricted on the flank of the topographic high of the Gargaf Formation. The faults in the central area also showed an influence of the thickness variation on the Waha Formation. Figure 10a indicates that the crest of the structural closure in the study area is at 1463 m (4800 ft), the maximum structural closure observed is 244 m (800 ft), and the maximum structural relief is approximately 457 m (1500 ft).

The structural model of the main zones of the Gargaf, Bahi, and Waha Formations provides the structural framework for reservoir property modeling. The combined structural, facies, and property models help us to understand how those reservoirs were stratigraphically and structurally connected. The constructed subzones of the Waha and Gargaf Formations were used to constrain the distribution of facies and property of reservoirs that were populated into the model. These subzones were further subdivided by adding layers to prepare the model for parameterization with geologic and reservoir properties (Figure 12a). The 3D grid has a horizontal

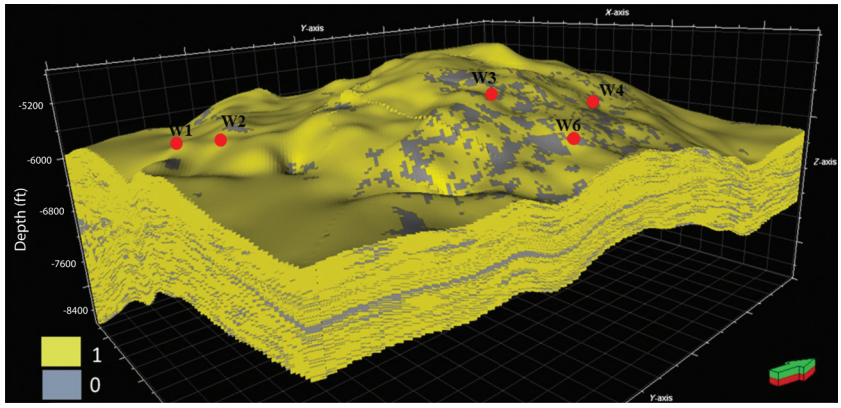

Figure 16. The 3D NTG ratio distribution of the Cambrian-Ordovician and Upper Cretaceous reservoir formations. The yellow or one represents the reservoir layer, and the gray or zero represents a nonreservoir layer.

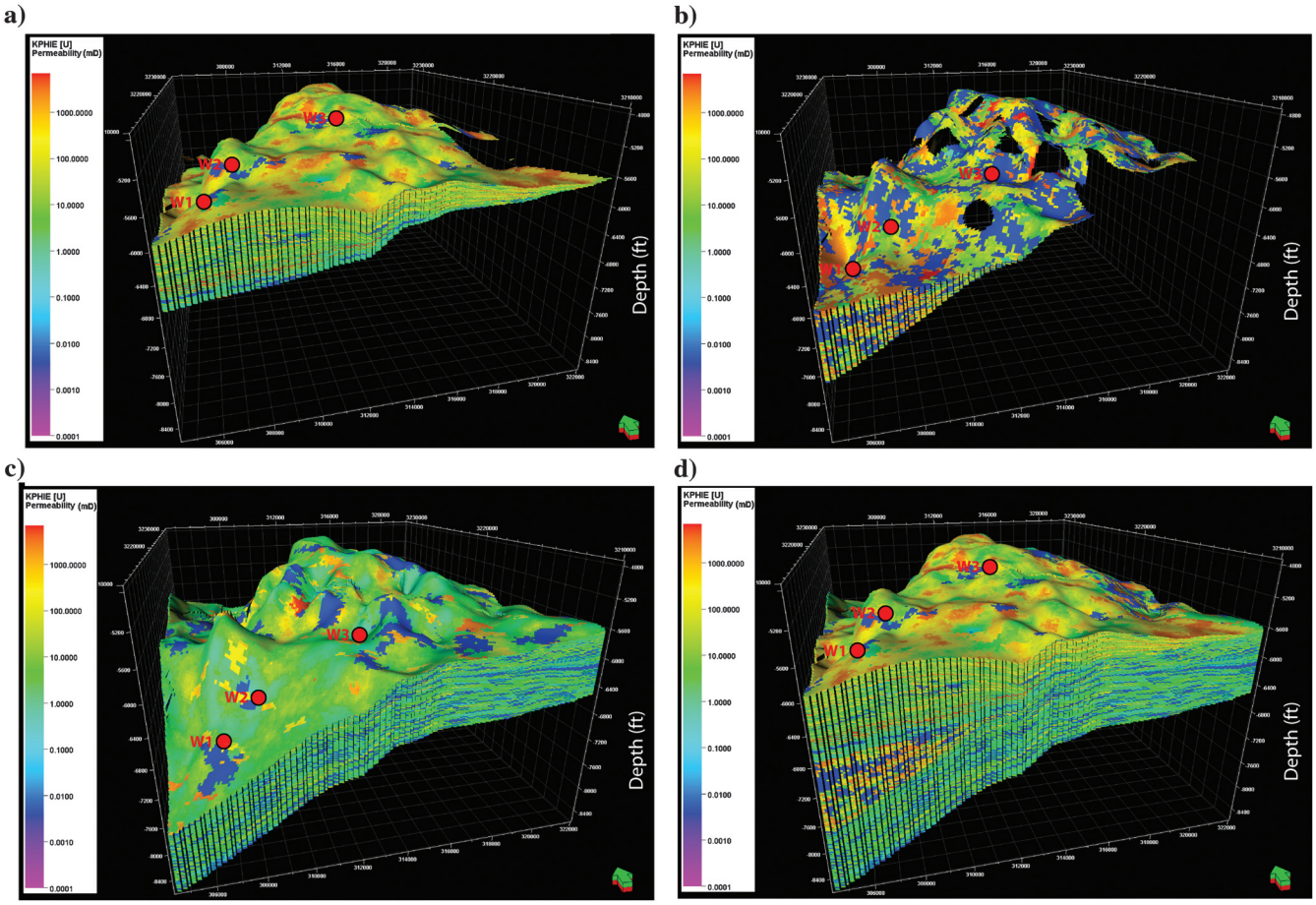

Figure 15. A 3D permeability model distribution of the Cambrian-Ordovician and Upper Cretaceous reservoir formations using the SGS. (a) The 3D permeability model of the Upper Cretaceous Waha Formation, (b) 3D permeability model of the Upper Cretaceous Bahi Formation, (c) 3D permeability model of the Cambrian-Ordovician Gargaf Formation, and (d) full-field 3D permeability model of the Waha, Bahi, and Gargaf Formations.

dimension of 16.9 km along the x-axis and 20.8 km along the y-axis, covering a surface area of 351.52 km^2.

Facies interpretation and modeling

We used well logs and core data to identify eight common facies, such as limestone, calcareous sandstone/sandy limestone, shale, sandstone, quartzite, conglomerate/boulder beds, shaly limestone, and dense limestones in the reservoir formations. Two other facies of argillaceous and sideritic limestone were also identified but in few wells. In addition to those facies, a nonreservoir facies that was characterized by impermeable zones was determined based on the resistivity cutoffs. The nonreservoir facies was indicated by a dark-gray area in Figure 13. The quality of the simulated model to well data for each facies and reservoir properties were checked using histograms. The resultant facies model of the Gargaf reservoir (Figure 13a) indicated that the quartzite facies is the most dominant facies in the Gargaf Formation in comparison with the sandstone and shale facies. The distribution of the nonreservoir zone is very limited and scattered in the Gargaf Formation.

The facies model of the Bahi Formation comprises siliceous sandstone, conglomerate, rare shale, and some limestone and calcareous sandstone facies. The reservoir is characterized by dominated facies of sandstone, with a relatively large portion of the nonreservoir zone. The nonreservoir facies has no effect on the hydrocarbon flow and reservoir connectivity, especially where the Bahi unit is characterized by thick deposits with high porosity in the southwestern part of the field. The variation of the Bahi facies does not compare to the distribution of porosity and permeability except for the large-scale variation of nonreservoir and reservoir facies. The combined facies and structural models suggested that the porous and permeable facies in the Bahi Formation tend to be in contact and hence permit transmitting fluids between the overlying and underlying reservoirs of the Bahi Formation. The connectivity of the reservoirs might also be enhanced by faults, where the high porosity and permeability of the Gargaf Formation were encountered in the central area.

The Upper Cretaceous Waha Formation comprises calcareous sandstone, limestone, and shale. Argillaceous and sideritic limestones have significant thicknesses in only a few wells. The constructed facies model of the Waha reservoir (Figure 13a) indicated that the dominant facies were limestone and calcareous sandstone and rare sandstone. The distribution of those facies varies in each subzone in the Waha Formation without a definite pattern. Nevertheless, the calcareous sandstone and shale contents tend to increase toward the northern and southern areas, respectively. The nonreservoir zone in respect to the other facies in the Waha Formation is very rare and is scattered in the subzones.

Porosity and permeability modeling and NTG ratio and volumetric estimation of the hydrocarbon resources

The porosity model of the basal fractured Gargaf quartzite unit shows that the average porosity, not including the fractures, is 2%, and the average permeability is less than 0.1 md. However, in the middle of the producing area, the Gargaf Formation shows relativity high porosity and permeability, where the porosity reaches 10%, and the permeability reaches 0.55 md (Figures 14 and 15). We also found that the porosity of the Bahi conglomeratic sandstone decreases with depth and thickness. The porosity of the Bahi ranges from 5% in the southeastern part to 30% in the southern and southwestern parts of the field, an area in which the Bahi is thicker than 46 m (150 ft). We found that the porosity in the Upper Cretaceous Waha Formation ranges from 15% in the southern part of the field to 25% in the northern part. The permeability ranges from 10 to 350 md and up to 2000 md in which the Waha and Bahi Formations exhibited higher permeability than the Gargaf Formation.

The final grid required for the 3D geologic model is the NTG model. NTG values range from zero to one in a reservoir rock. The NTG ratio of the Cambrian-Ordovician and Upper Cretaceous reservoir formations is 1.0 in most of the field. All of the wells in the study area are vertical, penetrating the base of the pay zone. The lateral and vertical variations observed regarding the NTG ratio are limited, which makes generating separate variograms for the description of these minimal variations in the NTG ratio meaningless (Dashti et al., 2013).

The OWC and the GOC are at 1676 m (5500 ft) true vertical depth (TVD) and 1539 m (5050 ft) TVD, respectively (Figure 17). Despite large lithologic variations and faulted and fractured zones of the reservoirs, the structural closure has a single hydrocarbon accumulation that was defined by two contacts from most of the old wells. The absence of the reservoir compartments and unified OWC and GOC contacts in the field can be explained by the distribution of simulated facies, reservoir properties, and NTG models of the reservoirs. The faults seem to facilitate the fluid flow conductivity and slightly control the thickness variation of some reservoir units. Based on our hydrocarbon volume estimate, we found that the largest hydrocarbon volumes were in the Upper Cretaceous Waha Formation. The total OOIP

Table 1. Volumetric estimation for the Cambrian-Ordovician and Upper Cretaceous reservoir formations after modeling each zone.

Formation	Bulk volume (10^6 RB)	Net volume (10^6 RB)	Pore volume (10^6 RB)	HCPV oil (10^6 RB)	OOIP (10^6 RB)
Waha	25,176.6	25,176.6	3727.8	2466.3	1644.3
Bahi	2850.1	2850.1	209.4	156.2	105.1
Gargaf	42,724.1	42,724.1	1781.0	1198.4	799.1

HCPV, hydrocarbon pore volume.

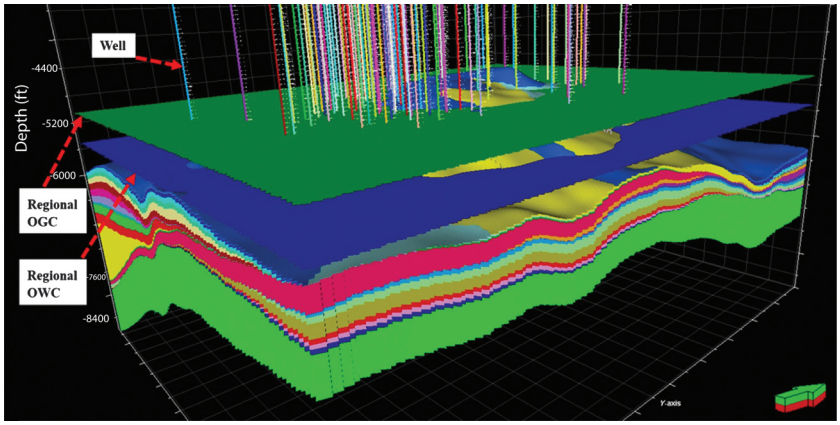

Figure 17. The 3D structural model showing the identified fluid contacts, the regional GOC at 1539.2 m (5050 ft) (the green surface), and the regional water-oil contact at 1676.4 m (5500 ft) (the blue surface). Columns in the middle indicate the wells.

for the full field model is estimated to be 2.55×10^9 stock tank barrel (STB), which is significantly higher in the last published estimation of approximately 2.05×10^9 STB (Brennan, 1992).

Conclusion

The constructed full-field static model of the Cambrian-Ordovician and Upper Cretaceous reservoirs helps to estimate hydrocarbon volumes and to understand reservoir heterogeneity and the main controlling factors on the distribution, thickness variation, and quality of the reservoirs. The porosity, permeability, water saturation, and a total of nine facies of the reservoir units were petrophysically determined and modeled using geostatistical modeling techniques. The most common facies in the reservoirs are (1) limestone and calcareous sandstone facies in the Waha Formation, (2) siliceous sandstone in the Bahi Formation, and (3) quartzitic sandstones in the Gargaf Formation. The resultant structural and isochore maps for the main producing formations suggest that the preexisting high structure of the Gargaf Formation seems to predominantly affect the spatial distribution of the Waha reservoir, and faults appear to mostly control the patchy distribution and thickness of the Bahi reservoir. The three reservoirs were connected by a total of 20 faults, and the reservoir structure with a maximum relief of 457 m in the oil field was formed and defined by major faults F1 and F2 with a throw of 250 and 130 m, respectively.

The widely expanded quartzite facies with poor reservoir quality (except in the fractured regions in the middle of the producing area) characterizes the Gargaf reservoir in the study area. The fractures in the Gargaf reservoir might have formed during the formation of the Gargaf paleohigh and were enhanced during the Cretaceous faulting. Siliceous sandstones and boulder beds of the Bahi Formation were recognized from cores and distinguished using neutron porosity logs based on the porosity variation. The former was characterized by a higher porosity than that found for quartzitic facies of the Gargaf, whereas the latter facies was characterized by lower porosity. A patchy zone of relative high porosity and permeability of the Bahi Formation exhibited better fluid conductivity in the thick section, whereas faults and the direct contact between the fractured Gargaf and Waha Formations facilitate fluid conductivity near the top of the structural closure. The Waha reservoir is characterized by two dominant facies of limestone and calcareous sandstone, which were distinguished using density-neutron crossplots. Despite the patchy distribution of both facies, the latter facies with better reservoir properties seems to be more common toward the northern part of the field, which agrees with an increase of the porosity values from 15% to 25% based on the porosity model.

The OOIP was estimated to be 2.55 billion barrels, among which more than 50% was found in the major Waha reservoir. The resultant model suggests that good quality areas of the Gargaf and Waha reservoirs tend to be around the main structural closure and are controlled by change of facies from dominant limestone to sandy limestone and the presence of faults and fractures. The resulting model can be refined with any new data and can be used with confidence for future development plans.

Acknowledgments

The authors wish to thank the National Oil Corporation Libya and the Sirte Oil Company for providing the information and data used in this study. We would like to thank the reviewers for their comments and suggestions that improved the work. The first two authors were sponsored by the Ministry of Education of Libya.

Data and materials availability

Data associated with this research are confidential and cannot be released.

References

Abadi, A. M., J. D. Van Wees, P. M. Van Dijk, and S. A. P. L. Cloetingh, 2008, Tectonics and subsidence evolution of the Sirte basin, Libya: AAPG Bulletin, **92**, 993–1027, doi: 10.1306/03310806070.

Abdelnabi, A., K. H. Liu, S. S. Gao, and Y. Abushalah, 2017, Seismic attributes aided fault detection and enhancement in the Sirte basin, Libya: 87th Annual International Meeting, SEG, Expanded Abstracts, 2340–2344, doi: 10.1190/segam2017-17431339.1.

Abushalah, Y., and L. Serpa, 2016, Using instantaneous frequency and colored inversion attributes to distinguish and determine the sandstones facies of the Late Ordovician Mamuniyat reservoir, R-field in Murzuq basin,

Libya: Interpretation, **4**, no. 4, T507–T519, doi: 10.1190/INT-2015-0167.1.

Abushalah, Y., and L. Serpa, 2018, Application of amplitude spectrum and genetic inversion to determine shaly facies distribution: A case study: Murzuq basin, Libya: Geophysical Prospecting, **66**, 1144–1158, doi: 10.1111/1365-2478.12627.

Adeoti, L., N. Onyekachi, O. Olatinsu, J. Fatoba, and M. Bello, 2014, Static reservoir modeling using well log and 3-D seismic data in a KN Field, offshore Niger delta, Nigeria: International Journal of Geosciences, **5**, 93–106, doi: 10.4236/ijg.2014.51011.

Ahlbrandt, T. S., 2001, The Sirte basin province of Libya Sirte-Zelten total petroleum system: U.S. Geological Survey, U.S. Geological Survey Bulletin, 2202-F, 29.

Al-Harbi, B., A. Al-Darrab, A. Al-Zawawi, and K. Al-Zamil, 2013, Advanced visualization for reservoir simulation: Presented at the SPE Saudi Arabia Section Technical Symposium and Exhibition.

Anketell, J. M., 1996, Structural history of the Sirt Basin and its relationships to the Sabratah basin and Cyrenaican platform, northern Libya, *in* M. J. Salem, A. S. El-Hawat, and A. M. Sbeta, eds., Geology of the Sirt basin: Elsevier 3, 57–88.

Asquith, G. B., D. Krygowski, and C. R. Gibson, 2004, Basic well log analysis: AAPG.

Baird, D. W., R. M. Aburawi, and N. J. L. Bailey, 1996, Geohistory and petroleum in the central Sirt Basin, *in* M. J. Salem, A. S. El-Hawat, and A. M. Sbeta, eds., Geology of the Sirt basin: Elsevier 3, 3–56.

Baric, G., D. Spanic, and M. Maricic, 1996, Geochemical characterization of source rocks in NC 157 block (Zaltan Platform), Sirt basin, *in* M. J. Salem, A. S. El-Hawat, and A. M. Sbeta, eds., Geology of the Sirt basin: Elsevier, 541–533.

Barr, F. T., 1972, Cretaceous biostratigraphy and planktonic foraminifera of Libya: Micropalaeontology, **18**, 1–46, doi: 10.2307/1484977.

Barr, F. T., and A. A. Weegar, 1972, Stratigraphic nomenclature of the Sirte Basin, Libya: The Petroleum Exploration Society of Libya.

Belhaj, F., 1996, Paleozoic and Mesozoic stratigraphy of eastern Ghadamis and western Sirt basins, *in* M. J. Salem, A. S. El-Hawat, and A. M. Sbeta, eds., Geology of the Sirt basin: Elsevier 1, 57–96.

Bellini, E., and D. Massa, 1980, A stratigraphic contribution to the Palaeozoic of the southern basins of Libya, *in* M. J. Salem and M. T. Busrewil, eds., Geology of Libya, London: Academic Press, 3–56.

Zou, Y., L. R. Bentley, L. Lines, and D. Coombe, 2006, Integration of seismic methods with reservoir simulation, Pikes Peak heavy-oil field, Saskatchewan: The Leading Edge, **25**, 764–781, doi: 10.1190/1.2210076.

Bezan, A. M., F. Belhaj, and K. Hammuda, 1996, The Beda formation of the Sirt basin, *in* M. J. Salem, A. S. El-Hawat, and A. M. Sbeta, eds., Geology of the Sirt basin: Elsevier 2, 135–152.

Bonnefous, J., 1972, Geology of the quartzitic "Gargaf Formation" in the Sirte basin, Libya: Bulletin du Centre de Recherches de Pau, Société Nationale de Petrole Aquitaine 6, 256–261.

Boote, D. R. D., D. D. Clark-Lowes, and M. W. Traut, 1998, Paleozoic petroleum systems of North Africa, *in* D. S. Clark-Lowes, ed., Petroleum geology of North Africa: Geological Society Special Publication 132, 7–68.

Boweman, J. N., 1962, Raguba field, Concession 20, Sirte Oil Company, unpublished report 96.

Brennan, P., 1992, Raguba field; Libya, Sirte basin, *in* E. A. Beaumont and N. H. Foster, eds., AAPG treatise of petroleum geology, Atlas of Oil and Gas fields, Structural traps VII 7, 267–289.

Cain, J. M., 2001, Geology and hydrocarbon potential, Concessions 16 and 20, Sirte Oil Company, unpublished report 250.

Capitanio, F. A., C. Faccenna, and R. Funiciello, 2009, The opening of Sirte basin: Result of slab avalanching?: Earth and Planetary Science Letters, **285**, 210–216, doi: 10.1016/j.epsl.2009.06.019.

Coward, M. P., and A. C. Ries, 2003, Tectonic development of North African basins, *in* T. J. Arthur, D. S. MacGregor, and N. R. Cameron, eds., Petroleum geology of Africa new themes and developing technologies: GSL, Special Publication 207, 61–83.

Craig, J., C. Rizzi, F. Said, B. Thusu, S. Luning, S. I. Asbali, and C. Hamblett, 2004, Structural styles and prospectivity in the precambrian and palaeozoic hydrocarbon systems of North Africa: 3rd Symposium Geology of East Libya, Binghazi, GSPLAJ; Extended Abstract, PETEX.

Dashti, L., E. Ma, M. Ibrahim, Y. Wang, S. Ryzhov, R. Al-Houti, and F. Abdulla, 2013, Answering the challenge of upscaling a 900 million-cell static model to a dynamic model greater Burgan field, Kuwait: Society of Petroleum Engineers, Middle East Oil and Gas Show and Conference, 249–4.

De Golyer, E. L., and L. Macnaughton, 2010, Engineering study, Concession 20, Sirte Oil Company, unpublished report.

Denney, D., 2013, Scaling up a 900-million-cell static model to a dynamic model: Journal of Petroleum Technology, **65**, 82–85.

El-Alami, M. A., 1996, Petrography and reservoir quality of the lower cretaceous sandstone in the deep Maragh trough, Sirt basin, *in* M. J. Salem, A. S. El-Hawat, and A. M. Sbeta, eds., Geology of the Sirt basin: Elsevier 2, 309–322.

El-Ghoul, A., 1996, An approach to locate subtle Waha structural on the Zaltan platform: Geology and geophysics, *in* M. J. Salem, M. T. Busrewil, A. A. Misallati, and M. J. Sola, eds., First symposium on the sedimentary basins of Libya, the geology of the Sirt basin: Elsevier 3, 137–154.

Futyan, A., and A. H. Jawzi, 1996, The hydrocarbon habitat of the oil and gas fields of North Africa with emphasis on the Sirt basin, *in* M. J. Salem, A. S. El-Hawat, and A.

M. Sbeta, eds., Geology of the Sirt basin: Elsevier 2, 287–308.

Gardner, G. H. F., L. W. Gardner, and A. R. Gregory, 1974, Formation velocity and density — The diagnostic basics for stratigraphic traps: Geophysics, **39**, 770–780, doi: 10.1190/1.1440465.

Gumati, Y. D., and A. E. M. Nairn, 1991, Tectonic subsidence of the Sirte basin, Libya: Journal of Petroleum Geology, **14**, 93–102, doi: 10.1111/j.1747-5457.1991.tb00301.x.

Gumati, Y. D., and S. Schamel, 1988, Thermal maturation history of the Sirte basin, Libya: Journal of Petroleum Geology, **11**, 205–218, doi: 10.1111/j.1747-5457.1988.tb00814.x.

Gumati, Y. D., and H. K. William, 1985, Early tertiary subsidence and sedimentary facies — Northern Sirte basin, Libya: AAPG Bulletin, **69**, 39–52.

Hallett, D., 2002, Petroleum geology of Libya: Elsevier, 503.

Hallett, D., and A. Ghoul, 1996, Oil and gas potential of the deep trough areas in the Sirt basin, Libya, the geology of the Sirt basin, *in* M. J. Salem, A. S. El-Hawat, and A. M. Sbeta, eds., Geology of the Sirt basin: Elsevier, 455–484.

Hamarbatan, N., A. Ajaily, and A. Hassan, 2006, High frequency imaging in an exploitation production environment — The Murzuq basin, case history: 68th Annual International Conference and Exhibition, EAGE, Extended Abstracts, doi: 10.3997/2214-4609.201402340.

Hamyouni, E. A., I. A. Amr, M. A. Riani, A. B. El-Ghull, and S. A. Rahoma, 1984, Source and habitat of oil in Libyan basins: Presented at the Seminar on Source and Habitat of Petroleum in the Arab Countries, Kuwait, 125–178.

Hassan, T., 1971, Waha distribution, Concession 20, Sirte Oil Company, unpublished report 151.

Heselden, R. G. W., J. M. Cubitt, P. Borman, and F. M. Madi, 1996, Lithofacies study of the Lidam and Maragh formations (Late Cretaceous) of the Masrab field and adjacent areas, Sirt basin, Libya, *in* M. Salem, A. J. Mouzughi, and O. S. Hammuda, eds., The Geology of Sirt basin,Proceedings of the 1st symposium, Sediment Basins of Libya 2, 197–210.

Hosseini, S. A., H. J. W. Lashgari, J. P. Choi, J. Lu Nicot, and S. D. Hovorka, 2012, Static and dynamic reservoir modeling for geological CO2 sequestration at Cranfield, Mississippi, USA: International Journal of Greenhouse Gas Control, **18**, 449–462, doi: 10.1016/j.ijggc.2012.11.009.

Johnson, B. A., and D. A. Nicoud, 1996, Integrated exploration for Beda formation reservoirs in the southern Zallah trough (west Sirt basin, Libya), *in* M. J. Salem, A. S. El-Hawat, and A. M. Sbeta, eds., Geology of the Sirt basin: Elsevier 2, 211–222.

Journel, A. G., and F. G. Alabert, 1988, Focusing on spatial connectivity of extreme valued attributes: Stochastic indicator models of reservoir heterogeneities: Presented at the SPE, SPE Paper 18324.

Journel, A. G., and E. H. Isaaks, 1984, Conditional indicator simulation: Application to a Saskatchewan uranium deposit: Mathematical Geology, **16**, 685–718, doi: 10.1007/BF01033030.

Kamali, M. R., A. Omidvar, and E. Kazemzadeh, 2013, 3D geostatistical modeling and uncertainty analysis in a Carbonate reservoir, SW Iran: Journal of Geological Research, **2013**, 687947, doi: 10.1155/2013/687947.

Karamitopoulos, P., G. J. Weltje, Q. Sacchi, and R. Dalman, 2013, Reducing the uncertainty of static reservoir models: Implementation of basin-scale geological constraints: 75th Annual International Conference and Exhibition, EAGE, Extended Abstracts, doi: 10.2118/164821-MS.

Klitzsch, E., 1971, The structural development of parts of North Africa since Cambrian time, *in* C. Gray, ed., Symposium on the geology of Libya, Tripoli: Faculty of Science of the University of Libya, 253–262.

Mansour, A. T., and I. A. Magairhy, 1996, Petroleum geology and stratigraphy of the southeastern part of the Sirt basin, Libya, *in* M. J. Salem, A. S. El-Hawat, and A. M. Sbeta, eds., Geology of the Sirt basin: Elsevier 2, 485–528.

Montgomery, S., 1994, Sirte Basin, north-central Libya: prospects for the future: Petroleum Frontiers: Petroleum Information Corporation.

Musa, F., D. Barr, M. Flynn, and M. Kalu, 2013, Modelling sub-seismic reservoir discontinuities: Integrating production data with seismic data and geological analogues: 6th International Petroleum Technology Conference.

Parsons, M. G., A. M. Zagaar, and J. J. Curry, 1980, Hydrocarbon occurrence in the Sirte basin, Libya, *in* A. D. Maill, ed., Facts and principles of world petroleum occurrence: Canadian Society of Petroleum Geology Memoir 6, 723–732.

Rodríguez Torrado, R., D. Echeverría-Ciaurri, U. Mello, and S. Embid Droz, 2015, Opening new opportunities with fast reservoir-performance evaluation under uncertainty, Brugge field case study: SPE Economics, and Management, **7**, 16–21, doi: 10.2118/166153-PA.

Roohi, M., 1996a, A geological view of source-reservoir relationships in the western Sirt basin, *in* M. J. Salem, A. S. El-Hawat, and A. M. Sbeta, eds., Geology of the Sirt basin: Elsevier 1, 323–336.

Roohi, M., 1996b, Geological history and hydrocarbon migration pattern of the central Az Zahrah-Al Hufrah platform, *in* M. J. Salem, A. S. El-Hawat, and A. M. Sbeta, eds., Geology of the Sirt basin: Elsevier 2, 435–454.

Rusk, D. C., 2001, Libya: Petroleum potential of the underexplored basin centers — A twenty-first-century challenge: AAPG Memoir, **74**, 429–452.

Schroter, T., 1996, Tectonic and sedimentary development of the central Zallah trough (West Sirt Basin, Libya), *in* M. J. Salem, A. S. El-Hawat, and A. M. Sbeta, eds., Geology of the Sirt basin: Elsevier 3, 123–136.

Sinha, R. N., and I. Y. Mriheel, 1996, Evolution of subsurface Palaeocene sequence and shoal carbonates, south-central Sirt basin, *in* M. J. Salem, A. S. El-Hawat, and A. M. Sbeta, eds., Geology of the Sirt basin: Elsevier 2, 153–196.

Van Houten, F. B., 1980, Latest Jurassic-earliest Cretaceous regressive facies, northeast African craton: AAPG Bulletin, **64**, 857–867.

Van Houten, F. B., 1983, Sirte basin, north-central Libya; Cretaceous rifting above a fixed mantle hotspot: Geology, **11**, 115–118, doi: 10.1130/0091-7613(1983)11<115:SBNLCR>2.0.CO;2.

Wennekers, J., F. Wallace, and Y. Abugares, 1996, The geology and hydrocarbons of the Sirt basin: A synopsis, *in* M. J. Salem, A. J. Mouzughi, and O. S. Hammuda, eds., The Geology of Sirt basin: Proceedings of the 1st Symposium, Sediment Basins of Libya 1, 3–56.

Abdalla Abdelnabi received a diploma (2000) in the petroleum industry from the Petroleum Training and Qualifying Institute, Libya; a B.S. (2005) in physics from Omar Al-Mukhtar University, Libya; a master's (2011) in geology and geophysics from the Missouri University of Science and Technology; a master's (2017) in petroleum engineering from the Missouri University of Science and Technology; and a Ph.D. (2017) in geology and geophysics from the Missouri University of Science and Technology. He is member of SEG, AAPG, and SPE. His research interests include seismic interpretation, seismic attribute analysis, petrophysical analysis, and geologic and reservoir modeling.

Yousf Abushalah received a B.S. (1998) in geology from Al Mergib University, Libya; an M.S. (2008) in exploration geophysics from El Fatah University, Libya; and a Ph.D. (2016) in geophysics from the University of Texas at El Paso, Texas. He was employed by the OMV E&P Company in 2007 and joined the El Mergib University as a lecturer and research advisor in 2009. An expert in 2D/3D seismic interpretation integrated to G&G data, quantitative seismic interpretation (i.e., seismic inversion, rock physics, and amplitude variation with offset modeling), reservoir modeling, and seismic data conditioning and processing. His current research interests include modeling of seismic wavefield propagation and modeling and field testing of PS converted waves.

Kelly Liu received a B.S. (1984) in exploration geophysics from the China University of Petroleum and a Ph.D. (1998) in geophysics and space physics from the University of California, Los Angeles. She is a professor of geophysics at the Missouri University of Science and Technology. She is an elected fellow of the Geological Society of America and an associate editor for the *Journal of Geophysical Research: Solid Earth*. Her expertise includes 3D seismic data interpretation, digital signal processing and analyses, computational and observational seismology, and layered structure detection in the earth's mantle.

Stephen Shangxing Gao received a B.S. (1984) in marine geology and geophysics from the Ocean University of China and a Ph.D. (1995) in geophysics and space physics from the University of California, Los Angeles. He is a professor of geophysics at the Missouri University of Science and Technology. He was a postdoctoral research associate at the Carnegie Institution of Washington and served in the faculty of Kansas State University prior to joining Missouri S&T in 2006. He is a member of SEG and the American Geophysical Union, and he is an elected fellow of the Geological Society of America. So far he has published more than 90 peer-reviewed journal papers and approximately 220 conference proceedings or abstracts. His research interests include using P-to-S and S-to-P converted waves to image crustal and mantle discontinuities, crustal and mantle seismic anisotropy, and seismic tomography studies of the earth's interior.